Journal of Novel Applied Sciences
Available online at www.jnasci.org
©2019 JNAS Journal-2019-8-7/135-144
ISSN 2322-5149 ©2019 JNAS

Investigating the structure and characteristics of Sesquiplane wind turbine blades and determining the angle of deposition and wind speed to improve its performance with the help of CFD analysis

Rasool Mahmoudi[1*] and Nabil Waely[2]

1. MSc in Mechanical Engineering, Energy Conversion, University of Arvan Non-Professorship.
2. Ph.D. in Chemical Engineering, Dissertation Orienteering and Arendan Institute

***Corresponding author*:** Rasool Mahmoudi

ABSTRACT: Considering the importance of Sesquiplane wind turbines in generating electricity, a study of their efficiency has been considered. In this study, we examined the structure and characteristics of blades, and determining the angle of deposition and wind speed to improve its performance with the help of CFD analysis in order to optimize the production of electricity. Using CFD analysis, in this paper, a method Fast and accurate calculations for constant Permanent AOA are proposed based on the flow rate field data at two upstream reference points of the turbine blades. The new method can be used to compute and store AOA data during CFD simulations without the need for wide processing to analyze and optimize the aerodynamic efficiency of the turbine. Several reference and reference reference reference points were used to select the most suitable locations for two reference points for the AOA calculation, and it has been determined that by using flow data from two reference points in 0.5 atmospheres, the length of the chord upstream and the air far from each The HF can provide the most accurate assessment in a wide range of tested AOAs. Based on the proposed AOA estimation method, the performance of a fixed ground and VAWT variables of varying sinusoidal variables are compared. The analysis shows how the configuration of the sinusoidal rod can improve the overall turbine performance by maintaining more favorable AOAs, and increasing and distributing them.

***Keywords*:** Wind turbine blade, Sesquiplane, CFD analysis.

INTRODUCTION

Wind energy has been recognized as an important source of renewable energy due to environmental impacts and increased frequency in recent decades. Among the various wind turbine designs, the horizontal-axis wind turbine (HAWT) is the most common in the world [1]. The main purpose of wind turbine design is to improve energy production and reduce wind energy costs. For this reason, various techniques have been developed, one of the most important of which is to effectively and efficiently increase the rotor's turbine wind power [2]. Wind turbines of a few megawatt rotors are usually 80 to 150 meters in diameter, and in super-cases up to 180 meters and single-blade lengths up to 88.4 meters [3].

The future of wind turbines is expected to continue in the future [4]. However, the development of large blades has challenged the difficulty, weight and cost of advanced materials. As the blade length increases, nail deviation increases rapidly. To ensure rigidity and avoid spatial interference between the blade and the tower, the blades should be produced with thicker fiberglass, which results in rapid weight gain. Under normal operating conditions, the tip of the traditional blade is typically 3 to 10 percent longer than the blade, and can be in the extreme conditions

of 15 to 20 percent [5]. Industrial safety standards for wind turbines usually require at least a distance of 30% between the tower and the tip of the constant blade while moving the rotor [6,7].

According to the safety factor, the tower-to-tip spacing should be about 20 to 25 percent of the blade length, which makes the nacelle's very fatal moments. Different methods have been used to prevent strike strikes, which are generally divided into two ways: increasing the tip clearance and increasing the stiffness of the blades. The first approach involves directly adjusting the rotor position (rotating the rotor so that the blades rotate upwards from the tower to the angle), propel the rotor and advance the blade [8, 9].

In application, this approach may have additional deficiencies and challenges, such as excess load and axial torque in the frigate, reducing aerodynamic efficiency, higher cost of blades and bearings, and increasing transportation and booking problems. Another problem with this method is that the hardness, vibration and fatigue characteristics of the blade remain unchanged, although long blades require a higher rigidity and low weight to combat the increased fatigue load and prevent escalation of tower passage Have a periodic presence. On the contrary, the second approach focuses on improving hardness with advanced materials and production processes, or an optimal design of personal blades and blade formation. Research on carbon fiber has focused on its high power and low density [10]. So far, the use of stronger materials is limited to a relatively small portion of large blades, but this allows for partial and partial reinforcement.

In the early years of air transport, balloon structures were widely used for structural advantages over single sonic or monophonic planes. The main advantage is that more rigidity can be achieved while keeping light weight simply increases structural depth. The two wings naturally make each other complicated for a conventional Mercedes-powered monopoly for their support. Also, lower wing loading in armor of a biopetric level will help even lighter wings, because less material is needed to achieve the same overall power. Length and thickness can also be small because the bioplastic surface has a large upper part and a good balance to balance the weight of the body. However, due to the aerodynamic interference between the two wings, a double lift can not double the rise of a similar size monopole. The previous wind tunnel test on the isomeric micro-airplane (MAV) isometric biomass in the lifting range of 64- 158% at low angles (less than 10 degrees) and at 30-66 percent at high angles (more than 10 degrees) compared to a monoplane , Where the ratio of the distance and the winged wing of the two-sided pillow was 0.533 [11]. Additionally, the biosphere wings were considered as high-speed high-speed configuration, [12] which limits the improvement of performance. The above factors cause the explosion of a two-dimensional aircraft in the late 1930s when structural materials and techniques were improved and high speed became a key requirement for airplanes; note that at low speeds, the effect of interference and the removal of columns, relatively modest factors And it was acceptable. Even in the modern aerospace industry, billboard configuration is still worth it. Studies conducted over the past 30 years show that the bells can be more efficient than monoplane with a proper gap, deviations and rotation [13-15]. In short, we can find three main reasons for the emergence and popularity of the dubbed aircraft:

In the current wind turbines, you can see a great similarity between the wings and wind blades. Techniques and costs of finite materials limit further development of long blades, and wind turbines operate at the same speed range as twin planes. The Fiat CR42B's body in 1941 can reach a maximum speed of 323 mph (144.4 m / s), [16] which is close to the usual speed of the tip of the blade tungsten. In other words, it's normal to assume that the Bridge Bridge configuration is also suitable for wind turbine blades. Nevertheless, it is important to recall that another role of billboard configuration on the aircraft was as a means of increasing lifters, where the configuration of the isometric biomolecule was appropriate to short short panels; in wind turbines, blades are usually very long And the stiffness (rather than lifting) is the main goal. An isometric two-dimensional structure that doubles the weight of the blade. In order to exploit the advantages and eliminate the shortcomings of a bridging structure, an anisometric two-sided blade structure is formed, as shown in Fig. 1. The main pair of the current blade will not change. The hardware belts are aligned with the original motor, and are significantly smaller than both the distance and the chords. The key to configuring the sesquiplane is to maintain the structural benefits of Bridge Bridge and reduce congestion.

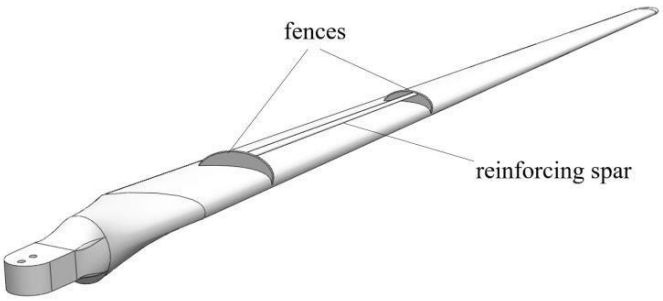

In very long blades, multiple couplings of fences and hard belts can be mounted adjacent to the blade's half-base, which is the most loaded. In the case of a single rotation, two fences are connected to the main gear, which acts as a connection between the original gear and the bending rotation. Fences can be made as an original piece or made to a single piece or, if necessary, mounted on the coating layer around the main gear surface. To ensure aerodynamic efficiency, the entire reinforced structure is well designed with aerodynamic features: the wing section is an airplane, and the fences are like borderline fences that prevent air flow. As the surface and volume of hardcoders and fences are smaller than the original pair, materials of high intensity and high intensity, such as carbon fiber composite materials, are recommended for rotation of stiffness, which significantly increases the integrity of the integral without increasing weight, and the cost . Both aerodynamic experiments and structural analysis were performed for design review.

Research methodology

The purpose of this study was to investigate the structure and characteristics of Sesquiplane wind turbine blades and determine the angle of deposition and wind speed for its performance improvement by analyzing CFD. In this research, the research method in terms of the purpose of the work is applied and in terms of the method of implementation is descriptive.

The criteria used in this study are the effect of the angle of deployment, wind speed and wind turbine blade properties, which is analyzed with the help of CFD analysis.

Physical range examination in terms of the angle of deposition, wind speed and atmospheric properties

The NREL Phase VI blade is used in this study as a blade for a twin wind turbine, which is a twisted and tapered blade shown in Fig. 1. The diameter of the 95-wind turbine rotor is 10,558 meters. The flow field is numerically simulated by reducing periodic boundary conditions to 96 computational costs.

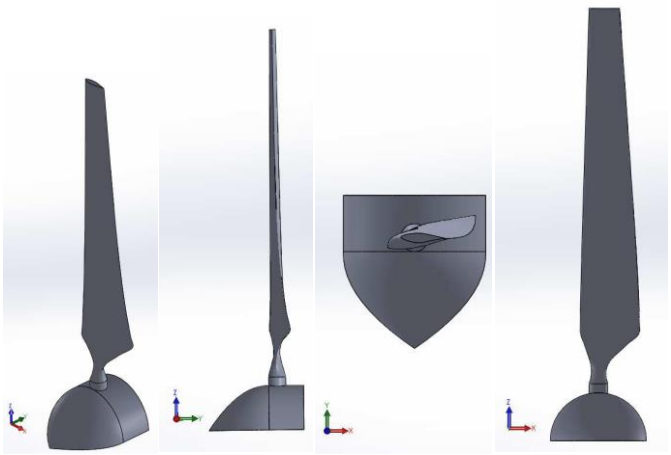

The flow around the wind turbine is considered as a non-condensing thick stream. 102 Therefore, 103 governing equations in the indirect form including continuity and complete reynolds equations of the new Stoic equations (RANS) in a rotating coordinate frame can be written as:

Symbols and equations for calculating the force applied to blades in wind turbines

A) Torque torque:

First state: In the case of movement of the motor and the base is constant. This mode is split into two times. In the event that the arm is accelerated, and in the absence of acceleration at steady-speed angles. It's likely that by drawing 360 degrees of motion, we realize that when we move 360 degrees at the beginning of the movement and accelerate the angular motion of the motor arm, at the end of this acceleration, both of which are non-zero values. Maximum anchorage is applied to the motor arm. We plot in the indeterminate presentation equations.

$$\alpha_{\text{r}} \quad \sum M_Z = I\frac{d}{dt}(\tau\ ACos\theta - P) = \circ$$

$$\omega_{\text{r}} \quad \sum \text{MX} = \text{I0}\Theta = 91190\ \times 0.014 = 1276.6\text{Nm}$$

$$\sum MY = I\Theta P = 152536 \times 0.014 \times 1.2 = 1562.6N.m$$

Force axis (X-Y-Z) is calculated.

Second state:

When the base moves. In this case, the motor is steady. This motion also has two non-accelerated states with fixed base angular velocity and base acceleration time, which is the first state because it is constant and is converted to a dignified state.

B) Motion analysis of the arm

In the static examination of the motor arm, other dimensions, other than length, are also effective. We have always made assumptions to simplify the analysis of the plate so we have to abandon these assumptions and make new assumptions for the analysis of the motor arm. For example, we have obtained the forces of bending and twisting around the hypothesis D, or the points C1 and C2 in the systematic section of the plate, in which we did not analyze the damage at that stage, but here we should see the center point of the plate (C2) And the end point of the motor arm (C1), since the distance between the center of the plate and the circular roller bearings is distant from the Cm40, and if the thickness of the rounded foam is also 20 cm2, the distance between C1 and C2 is 60 cm, which is non-There is also no point at all, and there is no other point at all, and the assumption is incorrect, but the surface is subjected to the thickness of the plate.

The torsional torque applied to the D at the end of the motor arm and converted to a transverse force in Z direction. The chosen path for xyz axes in solving motion is in the static solution of the motor arm and favorable paths. Therefore, the forces of the y path for the motor arm have the role of the axial stress and the moments of the z and y paths as the bending bend. The bending moments x and y are likely to apply the same fig as D onto the end of the motor arm. The torsional torque along the + y axis must be divided by a distance so that its transverse force is obtained on the motor arm in the Z path. In addition, this dynamic force has a static load due to the weight of the plate at the end of the motor arm.

In addition, the weight of the arm itself should be considered along the motor arm. It is likely that the forces resulting from the acceleration of the center side, which are applied due to the rotation of the base along the motor arm, are ignored because of the small size. The acceleration is very low. (Eric, 2008) There are no dedicated troops there. The width force entering Z is applied only to the upper side of the profile of the motor arm, and if we move it to the center axis of the beam, we will have a transverse force over the object in the x direction and a torque torque along the y axis. The jack force also enters the j point, and we also have the force of response to the de-b. The weight of the plate is divided into two components. A compressive and one-axis axis whose compression component, if placed on the middle axis of the armpit profile, will have a flexing moment on the X-path. We do not consider the axial force caused by the jack due to the small angle, ie, the jack is perpendicular to the axis of the motor arm, and we assume that its force is just the width. This assumption will be as bad as Jack's closing time.

First, let's take a look at the loads. In the event that the motor arm is lifted, a bending torque of N. m1276 is entered along the path x. And the twist torque N. m2562 also affects around D, which is transmitted to the surface of the contact between the rounded and movable arm and then transmitted to the center, and the matching of the torsion and transverse force is as follows.

$$\text{Fx}=\frac{2562N.m}{(1.46+60.8)n} = 1133N$$

This level is a force that extends transversely to the arm's length.

$$\begin{cases} M_x = -1276^{N.m} \\ F_X = -1133^{N} \end{cases}$$

The second is the time to accelerate the base. A bending torque in the x-axis bends as far as the motor arm, and a transverse torsional force enters the point D in the -x direction.

$$Fx=\frac{967}{2.26}=-428N$$

We also have a bending torque on the Z + path, bending it to the left and leveling it equal to

$$\begin{cases} M_X=-69367^{N.m} \\ F_X=-428^{N} \\ N_Z=1618^{N.m} \end{cases}$$

The third mode is the vertical movement of the device, which is solidly endorsed. This is the only dynamic force. Pleasures

The correctness of the (-) negative is confirmed by the right hand law for the three polarized P and M vectors.

Analysis of research findings

The finite element method has been used to analyze the structural characteristics of the Banacops blade. A simplified beam model has been used to calculate external deviations, as shown in Fig. 6. The monoplane brigade has been completed as a container beam, while the X-ray blades are attached as two asymmetric beams with two fingers. The beams pass through the blade's tensile centers. The amplifier parameter is 0.15 in the range of the blade (indicated by R), where the length is from 0 to 0.15R, the inter-hydraulic transmission and the blade blade. In order to compare the effect of the length of the amplification, the end of the variable ranged from 0.25R to 0.5R with an increase of 0.05R; it was believed that there was a big step of deviation. Slits in the mountain genital area are set as one of the main pairs. Material properties were taken from the SNL 100 blade [17]. For both monoplane and siccime rays, the hardness distribution and mass distribution along the blade length were calculated directly from the cross section. External loads are applied to models as distribution loads along the beams. Gravitational loads are calculated directly from the properties of the distributed beam mass. The beam model used by third-order Timoshenko elements. Aerodynamic loads are applied as static exterior loads, which were calculated using the theory of acceleration of the blade element in severe fatigue conditions specified by IEC 61400-1 [7]. The effect of the rotation of the aerial film was ignored because the angle of twisting for most blades was small. The blade range is adjusted to 100 m in order to indicate the direct tip.

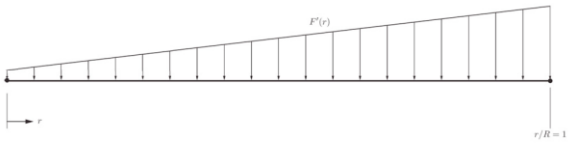

Suggested method for estimating AOA

In this paper, a new method for estimating AOA for VAWTs is proposed based on the flow field at two reference points above the turbine type. Since the ratio is close to the flow velocity and the direction to the blade is very complex and continuously changing, it is very important to determine the appropriate reference points in which the direction of the incident flare can be obtained for the correct estimation of the blade's AOA. To find these reference points around the blade, which can bring accurate and easy AOA calculations for VAWTs, fluid flow around a static plane with a range of set AOAs has been used as a test case. . The CFD simulation has been done to obtain flow field data around the Arrival at several selected reference points, and these data are used to compute the AOA around this static aerophole and compared with the AOAs set. Normal root square error (RMSE) is calculated based on the difference between the calculated and prescribed AOA and is used to select the most suitable reference locations with the minimum error, as discussed in Section 2.3. It has been found that using current data from two reference points in places of 0.5 longitudinal latitudes and upstream airfields and 1 air far from each side of the hurricane can be tested the most accurate estimates across a wide range of AOAs. Then, these selected reference locations are used to estimate the angle of attack around a VAWT blade, which is predicted well with AOA,

The proposed method for estimating AOA is shown in Fig.

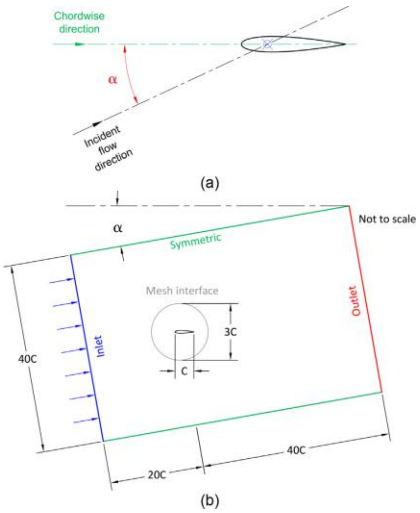

Conclusion

AOA Estimates for a Static Humidifier

The flow is around a static hovfile with a wide range of geometric AOAs as indicated in Fig. 2 (a), where NACA0015 Aerofil is used with 0.225m in length. This range of AOAs includes angles between 0 and 25 degrees with an increase of 5 degrees. The flow conditions and aerofoil geometry are selected according to the VAWT case, which is discussed in Section 3.1.1. Static acoustical simulations are carried out at various accidental speeds of 7, 14 and 21 [m / s], and this is a relatively moderate relative to the VAWT blade operating in TSRs 1, 2 and 3, the rotation in Main flow current at 7 m / s. This TSR range is tough to cover the optimal performance range of VAWTs. Due to the lack of empirical data in the selected flow conditions, data is widely used by the XFOIL software [40] to validate the CFD model. XFOIL has been designed to predict the Fayol air properties in Reynolds numbers. This is created by combining both integrals.

AOA Assessment Results for VAWT / VAWT Modeling

Model Results

Wind tunnel experiments, performed by Li and colleagues. [42], are selected to confirm the current CFD model. Their experimental data is a good opportunity to validate the CFD 2D simulation due to the inclusion of torque in the mid-section of the blade, based on the integration of momentary pressure data from a high-frequency multi-port scanner. In addition, their data includes the distribution of pressure around the wind turbine blade in various Asian locations. The experimental test was based on the VAWT model with two blades with a diameter of 1.7 mm. The blade is equipped with a NACA0015 with a length of 0.225 meters, a width of 1.02 meters, and a 4.5 4.5 ratio, and each external fixed blade of 6 degrees. In its experiments, a wind tunnel was used with an open section 3.6m. Measurements are found in a wind tunnel with an open test section, that is, without a wall around the test portion, to minimize the effects of obstruction [43].

The intensity of the turmoil in the test section was 0.5%. Details are available on the wind tunnel in [44]. For the selected test, the speed at the wind tunnel section was 7 meters per second, while the turbine rotated 180 rpm, and this gave the TSR 2.29

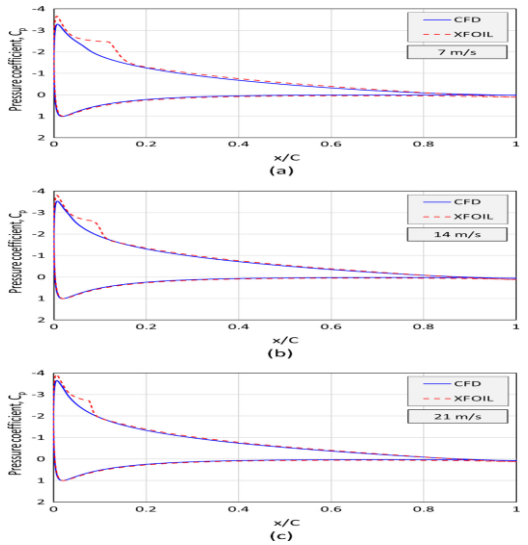

Figure: A comparison between CFD and XFOIL predictions of the pressure factor around aerofoil in AOA = 10 ° for flow velocity 7, 14 and 21 [m / s].

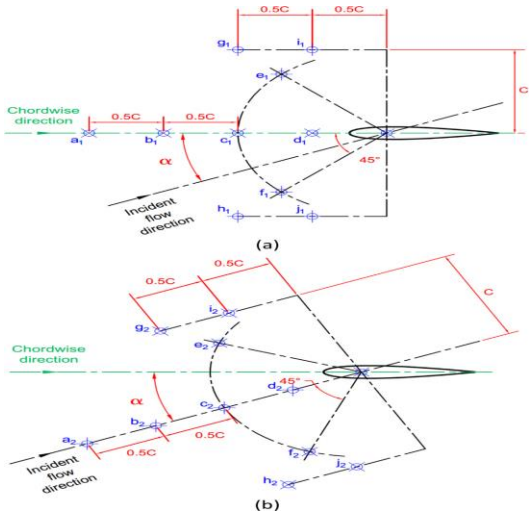

The flow around the plane of the VAWT semiconductor is modeled with a computational domain of Fig. Figure 10 shows the shape of the domain, sub-domains and different boundary conditions. The range of 8 diameters at the bottom of the rotation axis and 5 diameters otherwise, and the size of the range selected with good agreement, agrees in several recent studies [31,45,48]. The size of the domain is large enough to eliminate the effects of lateral and lower boundaries. ANSYS DesignModeler is used to mount the domain. The rear edge of the aerofoil has a radius of 0.19% to the chord, indicating a negligible effect on the aerofoil performance. However, the use of a rounded rear edge to prevent the prediction of accelerating flow over the sharp corners that surrounds the empty rear edge. In order to implement mesh grid method, the computational domain is constructed from several sub-domains. A circular spin sub-amplitude is associated with the area around the turbine with a diameter of 1.5 turbines diameter, while two small sub-amplitudes circle around the blade with a diameter of 2 ch in length are made at the request of the blade. Additionally, a large sub-domain representing a distant region of turbine and oil between these sub-domains passed through the non-uniform mesh mesh circle as shown in Fig.

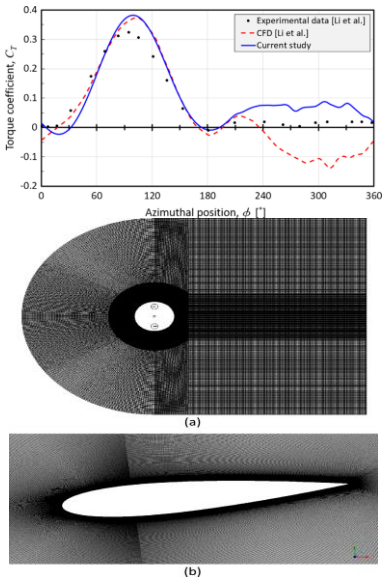

Figure - Shaped computing mesh is using ANSYS softwares to produce software and this mesh contains a combination of mesh O / C / H topology.

3.5 Results of the AOA Assessment for VAWT Ripples

A simple analysis of the AOA analysis, α is based on the assumption that the magnitude and direction of the approach to the wind, V, are constant and equal to the flow velocity generated by the flow, V∞. Figure 14 (a) shows the triangle of theoretical speed at the blade mounting point for a fixed constant zero turbine in an arbitrary azimuthal position, and φ and the velocity of the blade hardness is shown by TSR * V∞. Therefore, the relative speed of the local incident, Vr and AOA is simply defined as follows

$$V_r = V\sqrt{\sin^2\phi + (TSR + \cos\phi)^2}$$

$$\alpha = \tan^{-1}\frac{\sin\phi}{TSR + \cos\phi}$$

This AOA calculation is referred to as theoretical AOA. However, in real-world conditions, there are several phenomena that result in distortion in both the size and direction of the near-wind velocity vector. This involves expanding the streamtube, accelerating the flow in the turbine front and interfacing the wake through the blade. A triangular of realistic relative velocity can be seen by considering the magnitude and direction of approaching the wind speed as shown in the figure. A simple aerodynamic analysis can not provide accurate AOA prediction and relative velocity. However, detailed CFD data can provide a good estimate of these values, which can facilitate a better understanding of the turbine's performance.

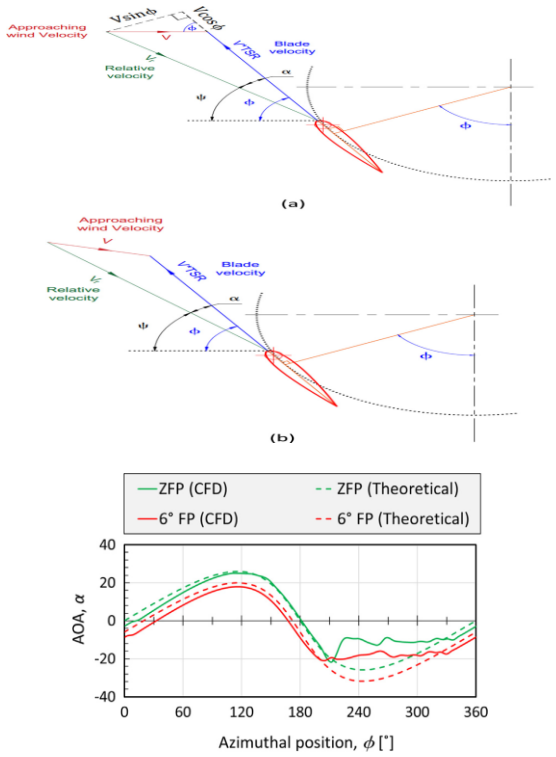

The moving speed between the reference point pair is calculated and averaged. Figure 15 shows that a comparison between the theoretical AOA obtained using equation (2) and AOA estimated by the proposed method is more than one cycle for both Zero Fixed (ZFP) and Fixed 6 (6) FP) that operate under the same conditions as the valid test. It is clear that the difference between the theoretical AOA and the AOA estimated in the upper part of the cycle is relatively smaller, that is, from 0 to 180 degrees of azimuthal angle, and these differences are expected to be due to the phenomenon of flow expansion. However, the difference in downstream cycles has increased dramatically.

REFERENCES

1. Yang Yanga, Pan Zenga,*, Liping Leia, (2018),Aero-structural Investigation of Sesquiplane Wind Turbine Blades, 10th International Conference on Applied Energy (ICAE2018), 22-25 August 2018, Hong Kong,China
2. M. Ansari, M.R.H. Nobari, E. Amani, (2019),Determination of pitch angles and wind speeds ranges to improve wind turbine performance when using blade tip plates, PII: S0960-1481(19)30431-8,DOI: https://doi.org/10.1016/j.renene.2019.03.119
3. Mohamed M. Elsakkaa,b, , Derek B. Inghama, Lin Maa, Mohamed Pourkashaniana, (2019), CFD analysis of the angle of attack for a vertical axis wind turbine blade, a Energy2050, Faculty of Engineering, University of Sheffield, UK, Faculty of Engineering, Port Said University, Egypt
4. M. Islam, S. Mekhilef, R. Saidur, Progress and recent trends of wind energy technology, Renewable and Sustainable Energy Reviews 21 .468–456 (2013)
5. O. Thomsen, Sandwich materials for wind turbine blades present and future, Journal of Sandwich Structures and Materials 11 (1) (2009) 7–26.
6. K. Bissonnette, Offshore wind assessment for the southeastern United States, Ph.D. thesis, Duke University (2016).
7. N. Fichaux, J. Beurskens, P. H. Jensen, J. Wilkes, S. Frandsen, J. Sorensen, P. Eecen, Upwind: Design limits and solutions for very large wind turbines, Sixth Framework Programme.
8. D. T. Griffith, T. D. Ashwill, The sandia 100-meter all-glass baseline wind turbine blade: Snl100-00.
9. G. W. Guideline, Guideline for the certification of wind turbines, Hamburg: Germanischer Lloyd Wind Energie Gmb H.
10. I. E. Commission, et al., Iec 61400-1: Wind turbines part 1: Design requirements, International Electrotechnical Commission.
11. A. Maqsood, T. H. Go, Parametric studies and performance analysis of a biplane micro air vehicle, International Journal Aeronautical and Space Sciences 14 (3) (2013) 229–236.
12. R. B. Addoms, Aerodynamic and structural design considerations for high lift biplane wing systems, 1971.

13. R. B. Addoms, F. W. Spaid, Aerodynamic design of high-perf romance biplane wings, Journal of Aircraft 12 (8) (1975) 629–630.
14. P. D. Gall, An experimental and theoretical analysis of the aerodynamic characteristics of a biplane-winglet configuration. md thesis.
15. R. L. Roedts II, Design of a biplane wing for small-scale aircraft, in: 47th AIAA Aerospace Sciences Meeting Including The New Horizons Forum and Aerospace Exposition, 2009, pp. 5–8.
16. Islam MR, Mekhilef S, Saidur R. Progress and recent trends of wind energy technology. Renew Sustain Energy Rev May 2013;21:456–68.
17. Marten D, Bianchini A, Pechlivanoglou G, Balduzzi F, Nayeri CN, Ferrara G, et al. Effects of airfoil's polar data in the stall region on the estimation of Darrieus wind turbine performance. J Eng Gas Turbines Power 2016;139(2):1–9.
18. Tjiu W, Marnoto T, Mat S, Ruslan MH, Sopian K. Darrieus vertical axis wind turbine for power generation II: Challenges in HAWT and the opportunity of multi-megawatt Darrieus VAWT development. Renew Energy 2015;75(March):560–71.
19. Bhuyan S, Biswas A. Investigations on self-starting and performance characteristics of simple H and hybrid H-Savonius vertical axis wind rotors. Energy Convers Manage 2014;87(November):859–67.
20. Bhattacharjee S, Acharya S. Performative analysis of an eccentric solar–wind combined system for steady power yield. Energy Convers Manage 2016;108(January):219–32.
21. Ghasemian M, Ashrafi ZN, Sedaghat A. A review on computational fluid dynamic simulation techniques for Darrieus vertical axis wind turbines. Energy Convers Manage 2017;149(October):87–100.